

See discussions, stats, and author profiles for this publication at: <https://www.researchgate.net/publication/231667219>

# Role of Surface Structure on the Charge Trapping in TiO<sub>2</sub> Photocatalysts

ARTICLE *in* JOURNAL OF PHYSICAL CHEMISTRY LETTERS · OCTOBER 2010

Impact Factor: 7.46 · DOI: 10.1021/jz1013246

---

CITATIONS

22

---

READS

25

2 AUTHORS, INCLUDING:



Matthias Batzill

University of South Florida

116 PUBLICATIONS 4,341 CITATIONS

SEE PROFILE

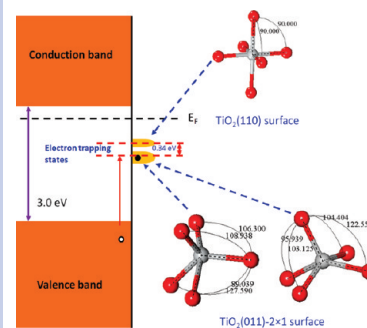
# Role of Surface Structure on the Charge Trapping in TiO<sub>2</sub> Photocatalysts

Junguang Tao and Matthias Batzill\*

Department of Physics, University of South Florida, Tampa, Florida 33620, United States

**ABSTRACT** Surface reconstruction of the rutile-TiO<sub>2</sub>(011)-2 × 1 surface places Ti ions in a distorted square pyramidal coordination environment. This variation of the crystal field compared to the common octahedral symmetry causes the binding energy for excess electrons, occupying Ti 3d states, to be 0.34 eV higher for the (011)-2 × 1 surface compared to that for the (110) surface. The role of adsorbates in the formation or annihilation of excess charges in TiO<sub>2</sub> is studied on the example of acetic acid adsorption. We find that bridge bidentate adsorption on the (110) surface results in extraction of excess charges from the substrate, while monodentate adsorption on the (011)-2 × 1 surface causes net-charge donation to the substrate. Differences in adsorbate-induced charge donation and, more importantly, binding energy differences of excess charges for the two surfaces may explain the face-dependent photocatalytic activity of rutile TiO<sub>2</sub>.

SECTION Surfaces, Interfaces, Catalysis



**T**iO<sub>2</sub> has become one of the most intensively studied photochemical materials because of its applications for the remediation of pollutants and solar energy conversion.<sup>1–3</sup> On rutile TiO<sub>2</sub>, face-dependent photoactivity has been observed,<sup>4–6</sup> with the (011) surface exhibiting a stronger activity toward oxidation reactions than the (110) surface.<sup>6</sup> The origin of this face dependence is not fully explained and only recently was the structure of the (011)-2 × 1 resolved.<sup>7,8</sup> The complex surface reconstruction of the (011) termination has striking structural features. Importantly, the Ti ions are in a unique Ti–O coordination environment. As shown in Figure 1a, c, and d, the Ti coordination in the surface is described by a distorted square pyramidal structure rather than the usual octahedral symmetry in the bulk or at other surfaces, such as (110) surface shown in Figure 1b. Consequently, this surface structure gives rise to a different crystal field at the surface titanium sites. Although there has been no measurable difference in the electronic structure of the stoichiometric (011)-2 × 1 reconstructed surface compared to other TiO<sub>2</sub> surfaces, that is, no specific surface states have been observed, one may expect the crystal field to be important if excess charges are placed on the Ti ions, that is, if the Ti<sup>4+</sup> ions are partially reduced to Ti<sup>3+</sup>. Such excess charges may be introduced by charge-donating defects or adsorbates, such as O vacancies (O<sub>vac</sub>) or surface hydroxyls (–OH), or may originate from photoexcited charge carriers relevant in photocatalysis.

Excess-charge-induced Ti 3d states within the band gap of  $\text{TiO}_2$  have been studied extensively on the (110) surface. Each  $\text{O}_{\text{vac}}$  introduces two excess electrons that are transferred to the empty Ti 3d orbitals, which is verified by resonant photoemission studies.<sup>9,10</sup> From ultraviolet photoemission spectroscopy (UPS),<sup>9</sup> a band gap state (BGS) about 0.9 eV below the Fermi level ( $E_F$ ) is observed for slightly reduced

surfaces. This BGS has long been correlated with electron-donating surface defects such as  $O_{\text{vac}}$ <sup>11</sup> or  $-\text{OH}$ .<sup>12</sup> Recently, however, subsurface Ti interstitials have been proposed as an alternative origin of the BGS.<sup>13</sup> In addition to the origin of the BGS, the distribution of these excess electrons is also debated. Both a localization of excess electrons at Ti atoms close to the electron donor defect as well as delocalization over many Ti sites, including subsurface Ti sites, are discussed. Theoretical calculations alone have failed to address these issues decisively due to the limited ability to treat the localization of electron states inside of the band gap. Depending on the approximation used for the exchange and correlation potentials, some conflicting conclusions have been reached. Pure density functional theory (DFT) calculations normally lead to a delocalized nature of the excess charge,<sup>14</sup> while calculations based on the Becke three-parameter Lee–Yang–Parr (B3LYP) functional predict that the electrons are localized on two specific surface Ti sites.<sup>15</sup>

Here, we use photoemission spectroscopy to compare experimentally the BGSs at the (011)-2  $\times$  1 and (110) surfaces of rutile TiO<sub>2</sub> and find that electron-donating defects introduce a BGS at different binding energies. This has far-reaching implications for electron trapping at these surfaces. Surfaces with a BGS at a higher binding energy imply a thermodynamically favored electron trapping. We propose that the more efficient trapping of charges may explain the reported varying photocatalytic activities of surfaces with different crystallographic orientation. In addition to trapping charges in the substrate, adsorbates may efficiently take up excess charges,

Received Date: September 23, 2010

**Accepted Date:** October 12, 2010

Published on Web Date: October 21, 2010

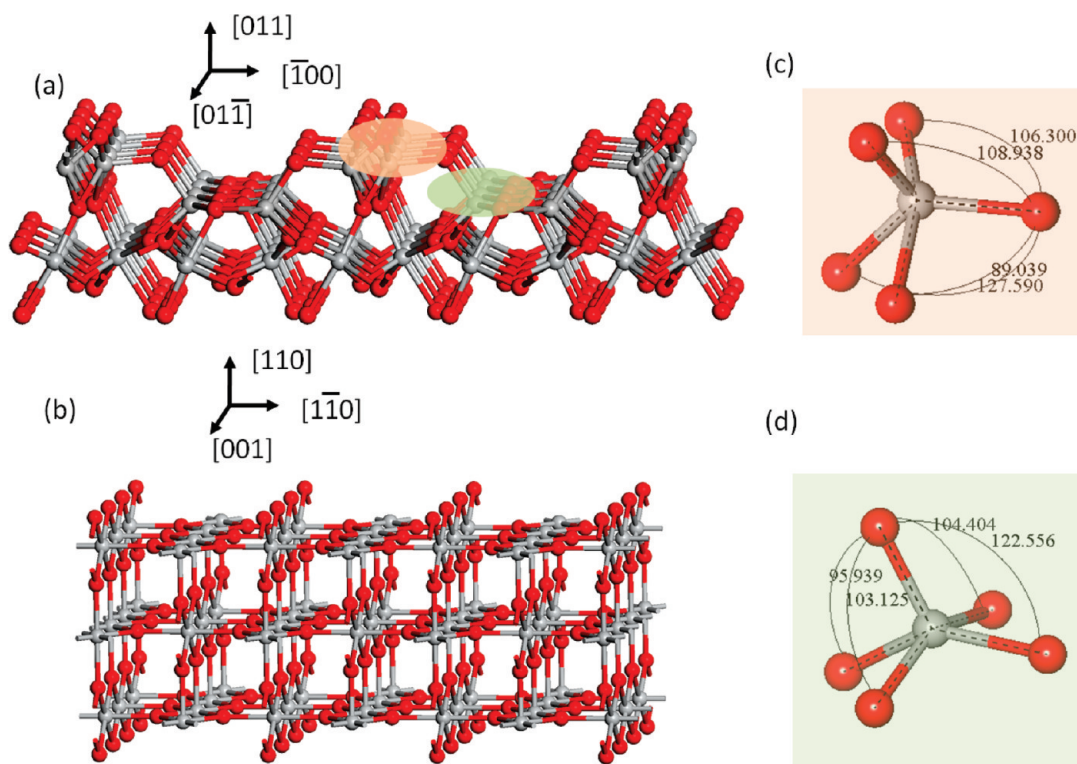


**Figure 1.** Ball-and-stick models for  $\text{TiO}_2(011)\text{-}2 \times 1$  (a) and (110) (b) surfaces. Gray and red spheres are Ti and O atoms, respectively. (c, d) Two different local Ti–O environments on the  $(011)\text{-}2 \times 1$  surface with the same color code as that specified in (a). The values shown in (c) and (d) are the bond angles.

and this charge transfer from the substrate to the adsorbate is central to surface photochemical reactions.<sup>16</sup> Here, we show, on the example of carboxylic acid adsorption, that the adsorption structure plays an important role in charge transfer from the substrate to the adsorbate, and thus, the surface structure is an important component in this process. Therefore, the two factors of excess charge relocation are strongly surface-structure-dependent, and thus, a better understanding of the relation between structure and charge transfer is important for designing better photocatalysts.

Figure 2a shows a STM image of a vacuum-annealed  $\text{TiO}_2(110)$  surface collected using a slightly reduced (light blue)  $\text{TiO}_2$  crystal. STM images were acquired with a tunneling current of 1.0 nA and a sample bias voltage of 1.2 V. The bright and dark rows correspond to surface five-fold Ti atoms ( $\text{Ti}_{5c}$ ) and two-fold bridging oxygen ( $\text{O}_b$ ) sites, respectively.<sup>17</sup> There are several bright spots between the bright rows which are attributed to surface-bridging O vacancies ( $\text{O}_b\text{-vac}$ ) or  $\text{-OH}$ , where the latter is formed by water dissociation at  $\text{O}_b\text{-vac}$  sites, as is typical for this surface. In contrast to  $\text{TiO}_2(110)$ , the STM image of a clean  $\text{TiO}_2(011)\text{-}2 \times 1$  surface exhibits rows of protrusions arranged in zigzag patterns, as given in Figure 2b. The bright spots in the STM image have been attributed to the geometrically protruding two-fold O ( $\text{O}_{2c}$ ) atoms arranged in a zigzag pattern along the  $[100]$  direction (see Figure 1a).<sup>18</sup> This surface exposes two different  $\text{Ti}_{5c}$  sites on the top and in the valley<sup>8,18</sup> in different distorted square base pyramidal coordination environments (see Figure 1).

In order to compare the energy position of defect states of both surfaces, UPS has been performed, and the corresponding spectra for  $\text{TiO}_2(110)$  and  $(011)\text{-}2 \times 1$  surfaces are presented in Figure 2c and d, respectively. In Figure 2c, besides the main feature of predominantly O 2p derived valence band states of bulk  $\text{TiO}_2(110)$ , the Ti 3d derived BGS (located  $\sim 0.9$  eV below  $E_F$ ) is clearly observed. On the vacuum-prepared  $(011)\text{-}2 \times 1$  surface, on the other hand, the BGS is very small (see Figure 2d). The BGS intensities are 1.9 and 0.17 % of the total valence band intensity for the (110) and (011) surfaces, respectively. This is consistent with the STM observations of fewer point defects on the  $(011)\text{-}2 \times 1$  surface compared to the (110) surface, which have been counted in STM images to typically amount to  $\sim 10$  and  $\sim 1$  % for (110) and  $(011)\text{-}2 \times 1$  surfaces, respectively. Therefore, the BGS intensity ratio in UPS agrees with the point defect density on these two surfaces. Furthermore, regardless of the “history”, that is, the vacuum reduction stage, of (110) samples, BGSs are always observed on this surface, while, as shown in Figure 2d, the  $(011)\text{-}2 \times 1$  surface can be easily prepared with a negligible BGS. This implies that surface point defects are a major contribution to the BGS. Therefore, we conclude that although UPS samples the first few nanometers of the surface region, subsurface defects, such as Ti interstitials, do not contribute significantly to the BGS observed in UPS. Our observations agree well with previous arguments that assign the BGS to electron-donating surface defects such as O vacancies and surface hydroxyl groups.<sup>11,19</sup> Exposing the (110) surface to  $\text{O}_2$  at room temperature is known to remove O vacancies as well

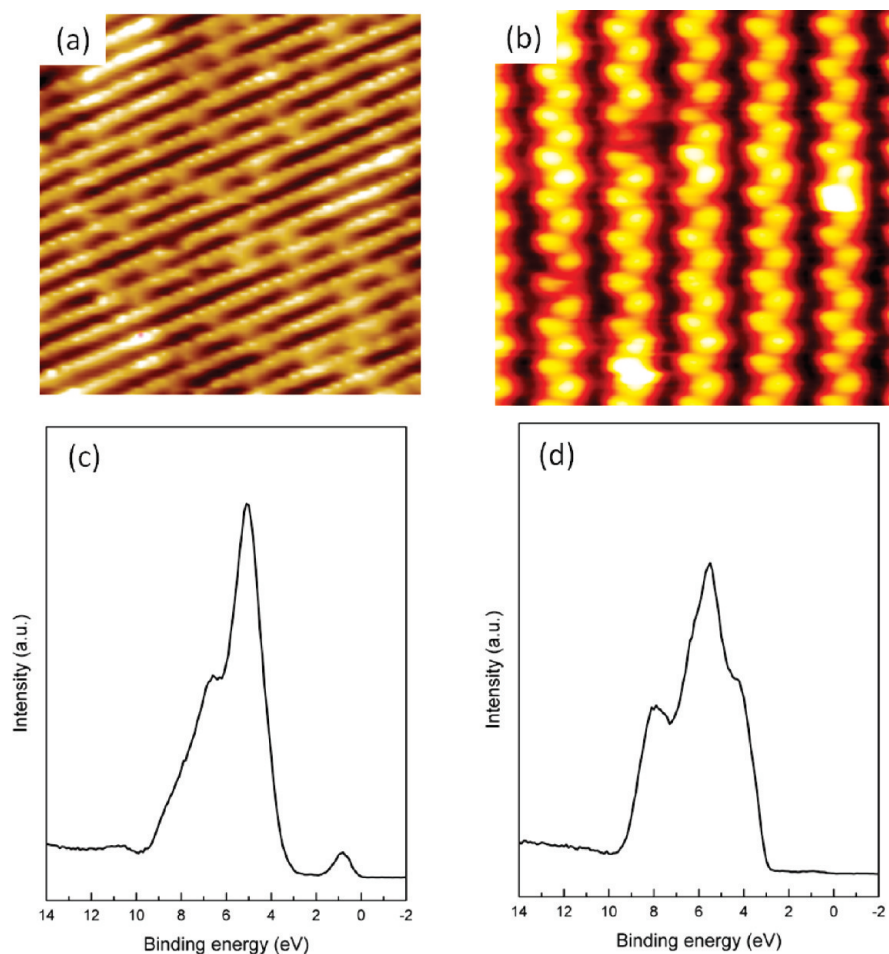


**Figure 2.** STM images of vacuum-prepared rutile surfaces; (a)  $\text{TiO}_2(110)$  ( $8 \times 8 \text{ nm}^2$ ) and (b)  $(011)\text{-}2 \times 1$  ( $4.8 \times 4.8 \text{ nm}^2$ ). The two bright spots in (b) are likely due to surface hydroxyls. The corresponding UPS spectra are shown in (c) and (d), respectively.

as hydroxyls.<sup>12,13</sup> Consequently, this process results in a suppression of the BGS on the (110) surface, as shown in Figure 3a. The remaining intensity ( $\sim 10\%$  of the original magnitude) may be attributed to contribution from sub-surface excess charges.

To investigate the effect that adsorbates may have on the defect states, we adsorb a carboxylic acid (acetic acid) at the surface. For the (110) surface, carboxylic acids are known to adsorb dissociatively, by splitting off the acetic hydrogen, in an ordered structure with a bridge bidentate adsorption on the  $\text{Ti}_{5c}$  rows.<sup>20–24</sup> In this process, the hydrogen is adsorbed on the two-fold bridging oxygen atoms at the (110) surface. The UPS spectra for (110) surface before and after acetate adsorption are shown in Figure 3b. As shown by the difference spectrum in the lower panel of Figure 3b, the acetate orbitals are mainly located at binding energies of  $\sim 10.4$ ,  $\sim 8.1$ , and  $\sim 5.7$  eV, which agrees, for example, with the reported values for bidentate adsorbed acetate on  $\text{Cu}(110)$  surfaces.<sup>25</sup> The higher binding energy peaks are dominated by the methylic carbon and carboxylic carbon orbitals, while the low binding energy peak originates from carboxylic oxygen atoms, which have direct bonding with the substrate through the oxygen lone pair.<sup>25,26</sup> In addition to the acetate molecules,

contributions from  $\text{OH}_\sigma$  are expected. However, the binding energy of the  $\text{OH}_\sigma$  bond overlaps with the acetate peak at  $\sim 10.4$  eV, and therefore, OH formation cannot be unambiguously confirmed from the UPS spectra. Figure 4a shows the  $2 \times 1$  ordered acetate superstructure on the (110) surface. Although the adsorbed hydrogen donates its electron to the substrate, the BGS on the (110) surface is decreased by  $\sim 40\%$  upon carboxylic acid adsorption; see Figure 3c. If acetic acid is adsorbed on an oxygen-pretreated surface, that is, a surface with a reduced BGS, the BGS is even completely removed within the detection limit upon adsorption of an acetic acid monolayer, as shown in Figure 3c. This indicates that on the (110) surface, the adsorbed acetate is taking up the charges donated from the adsorbed hydroxyls and other additional excess charges present at Ti sites prior to acetic acid adsorption. This contrasts the observations on the  $(011)\text{-}2 \times 1$  surface. Adsorption of acetic acid on  $\text{TiO}_2(011)\text{-}2 \times 1$  at room temperature also results in dissociative adsorption. STM shows the formation of hydroxyls as well as quasi-one-dimensional acetate clusters. At low acetate coverage, individual clusters are observed in STM as bright contrast features that are preferentially nucleated at surface defect sites, such as step edges and antiphase domain boundaries of the  $2 \times 1$



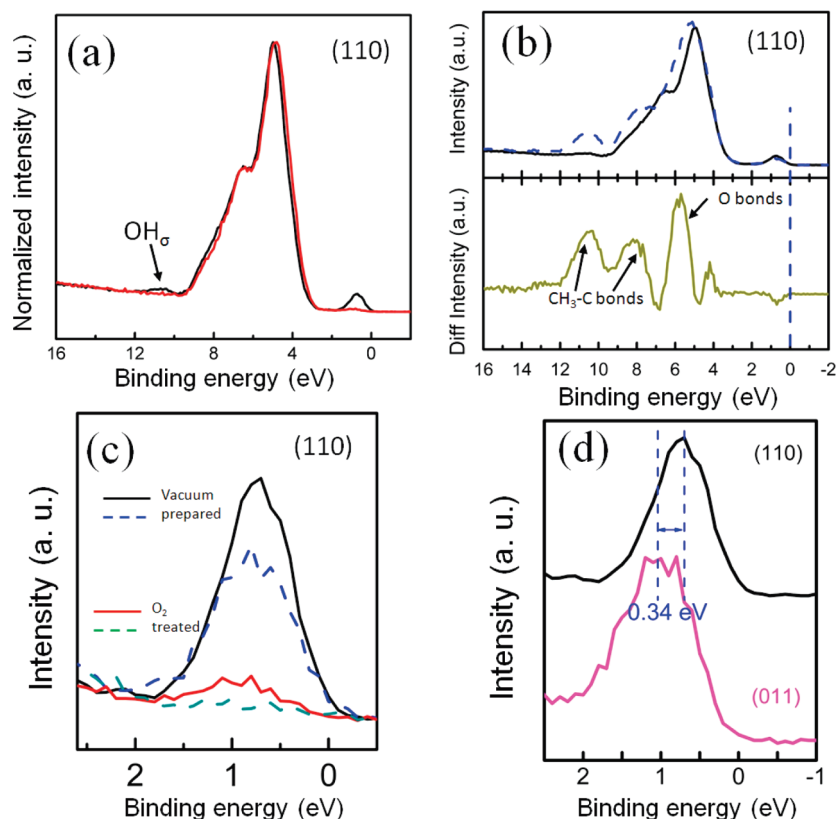


**Figure 3.** UPS valence band spectra on  $\text{TiO}_2(110)$ . (a) Exposure of the vacuum-annealed  $\text{TiO}_2$  surface (black curve) to  $\text{O}_2$  (red curve) results in a reduction of the  $\text{OH}_\sigma$  states and the Ti 3d BGS. (b) Valence band spectrum before (black solid curve) and after monolayer acetate adsorption (blue dashed curve). The difference spectrum between the clean and acetate-covered surfaces is shown in the lower panel of (b) (dark yellow curve). The change of BGS upon acetate adsorption is shown in (c) for vacuum-prepared and  $\text{O}_2$ -pretreated samples. The solid lines are before acetate adsorption, and the dashed lines are after adsorption. For both samples, a reduction in the BGS is observed upon acetate adsorption. In (d), the BGSs for the  $\text{TiO}_2(110)$  and  $(011)\text{-}2 \times 1$  surfaces are compared. The black curve is for the clean  $\text{TiO}_2(110)$  surface, and the pink curve is measured on the  $(011)\text{-}2 \times 1$  surface after acetate adsorption, when the BGS becomes noticeable. The BGS for the  $(011)$  surface is shifted  $\sim 0.34$  eV to higher binding energies compared to the  $(110)$  surface.

reconstruction; see Figure 4b. With increasing coverage, these clusters continue to grow in a strongly anisotropic manner in the  $[01\text{--}1]$  direction and eventually cover almost the entire surface, as shown in Figure 4c. Our temperature-programmed desorption (TPD) studies (not shown) demonstrated that these acetates are strongly bound to the surface and react to ketene at  $\sim 585$  K, similar to the reaction on the  $(110)$  surface. However, unlike the  $(110)$  surface, a bridge bidentate adsorption is geometrically impossible on the reconstructed  $(011)\text{-}2 \times 1$  surface, and acetate adsorbs in a monodentate configuration. This difference in the adsorption structure compared to the  $(110)$  surface is also reflected in the UPS spectra shown in Figure 4d. The high binding energy of the acetate molecular orbitals (10.4 eV), which is attributed predominantly to the methylic carbon and carboxylic carbon orbitals, is not significantly different compared to that of acetate adsorbed on the  $(110)$  surface. The molecular orbitals that are involved in the binding to the surface are shifted and are weaker in intensity compared to those of the  $(110)$  surface; most likely, this is a consequence of the lower symmetry of the monodentate adsorption configuration combined with a higher heterogeneity of the acetates in the clusters on the  $(011)\text{-}2 \times 1$  surface compared to that of the well-ordered

adsorption layer on the  $(110)$  surface. Interestingly, the BGS is increasing on the  $(011)\text{-}2 \times 1$  surface upon acetate adsorption, as shown in Figure 4d. This implies that the acetate is not able to take up all of the excess charge donated by the hydroxyls, leaving charges in Ti 3d states. This demonstrates that the coordination of the adsorbate to the substrate plays an important role for BGS in the substrate. Having two acetate–oxygen atoms coordinated to the  $(110)$  surface enables acetate molecules to overcompensate for the electrons donated by hydroxyl formation and consequently results in the observed suppression of the BGS. In contrast, coordination of only one oxygen atom of the acetate to the substrate on the  $(011)\text{-}2 \times 1$  surface leaves excess charges (donated by  $-\text{OH}$  groups) in the  $\text{TiO}_2$  substrate. Thus, we explain the amount of excess charge in the  $\text{TiO}_2$  substrate by the number of anionic ligands to the surface, that is, mono- versus bidentate acetate adsorption.

Comparing the BGS binding energies for the  $(110)$  and  $(011)\text{-}2 \times 1$  surface reveals that the binding energy for the  $(011)\text{-}2 \times 1$  surface is  $\sim 0.34$  eV higher than that for the  $(110)$  surface, as emphasized in Figure 3d. This is a significant energy difference for excess charges at Ti lattice sites and suggests that electrons are more effectively trapped on the

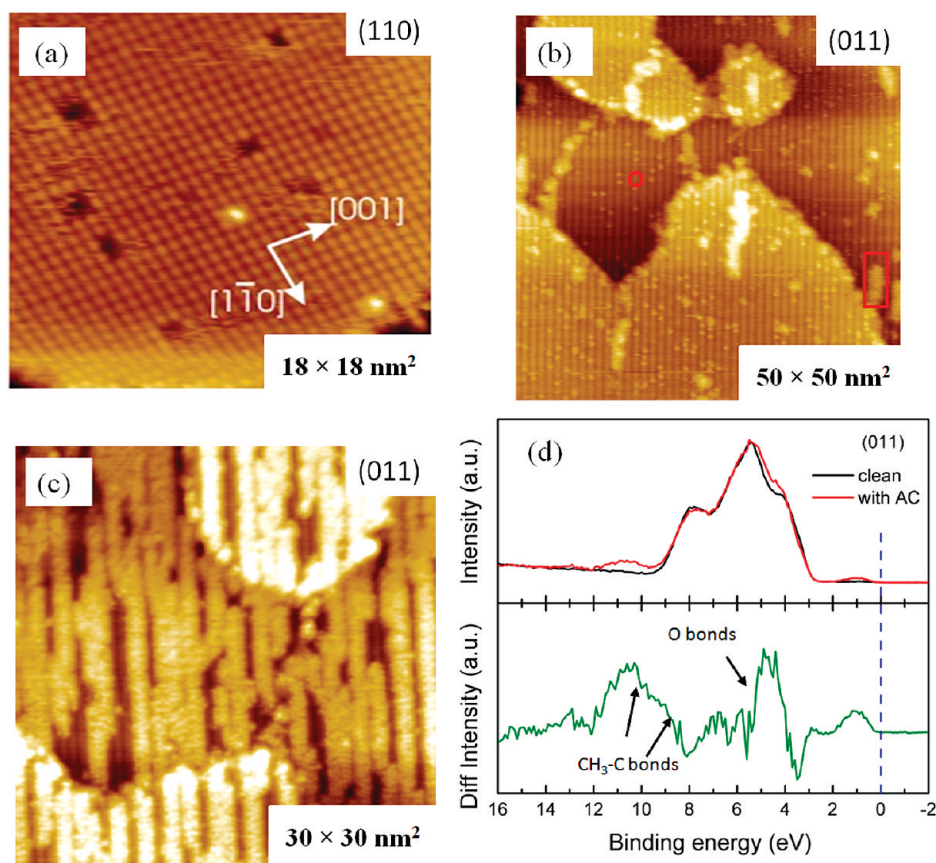


**Figure 4.** (a) STM image of saturated coverage of acetate on the rutile  $\text{TiO}_2(110)$  surface ( $18 \times 18 \text{ nm}^2$ ) showing a well-ordered  $2 \times 1$  adsorption superstructure. (b, c) The  $(011)\text{-}2 \times 1$  surface after acetate adsorption; (b) shows a ( $50 \times 50 \text{ nm}^2$ ) image with a low coverage of acetate. At low coverage, surface hydroxyls are easily discernible as point-like protrusions (one is indicated by the circle), while acetate forms clusters (indicated by the rectangle). Panel (c) shows a ( $30 \times 30 \text{ nm}^2$ ) image of the surface after high acetic acid exposure. At this coverage, the surface is densely covered by acetate clusters. The UPS spectra before (black curve) and after (red curve) acetate adsorption on the  $(011)\text{-}(2 \times 1)$  surface are shown in (d). The difference spectrum in the lower panel of (d) (olive curve) shows the acetate orbitals and the strong increase in the BGS upon acetic acid exposure.

$(011)\text{-}2 \times 1$  surface than on the  $(110)$  surface. We explain the higher binding energy of Ti 3d states on the  $(011)\text{-}2 \times 1$  surface by the geometry of the surface reconstruction and the resulting crystal field at the surface Ti sites. Due to the surface reconstruction, the Ti–O coordination environments at the  $(011)\text{-}2 \times 1$  surface are changed to two differently distorted square pyramid Ti–O coordination environments, as schematically shown in Figure 1c and d. Generally, a square pyramid coordination environment causes a larger crystal field splitting and stronger stabilization of the  $d_{xz}$  and  $d_{yz}$  orbitals compared to an octahedral configuration. Only Ti atoms in the topmost surface layer exhibit this unique coordination environment, and therefore, the observed higher binding energy of the Ti 3d state implies that the defect electrons are localized on the surface layer. The full widths at half-maximum (fwhm) of these defect states are  $\sim 1.0$  and  $\sim 0.8$  eV for the  $(011)\text{-}2 \times 1$  and  $(110)$  surfaces, respectively, which may be correlated with the fact that there are two different Ti–O coordination environments on the  $(011)\text{-}2 \times 1$  surface but only one on the  $(110)$  surface. The distribution for defect electrons on the  $(110)$  surface is still controversial,<sup>15,27</sup> and our implication of a localization in the surface layer of the

$(011)\text{-}2 \times 1$  surface may favor the description of localized charges. However, we cannot exclude that the charge localization depends on specific surface properties. In particular, it is possible that charges are more localized on the  $(011)\text{-}2 \times 1$  surface because of the unique crystal field for surface Ti sites, which energetically favor excess electrons to be located in the surface layer.

Other titania polymorphs, namely, anatase, also have slightly differing crystal fields compared to rutile. In anatase, the Ti sites are in distorted octahedral coordination, and the lower symmetry of these sites compared to that of the perfect octahedron of rutile will also increase the crystal field splitting. Indeed, the binding energy of BGS in anatase  $\text{TiO}_2$  is reported to be  $\sim 0.2$  eV higher than that in the rutile  $\text{TiO}_2(110)$  surface.<sup>28</sup> Therefore, this observation is in agreement with our simple model that the binding energy of the Ti 3d BGS is a consequence of the crystal field. More advanced electronic structure calculations would be desirable to confirm the relationship between crystal symmetry and band gap binding energy. Our experimental observations of differing binding energies of excess charges at the two  $\text{TiO}_2$  surfaces may provide an important test system for

benchmarking DFT computations. Reproduction of the BGS binding energy for the (110) and the reconstructed (011)-2 × 1 surface by DFT computations would be verification of the pseudopotentials and U parameters used in DFT computations.

The binding energy of excess charges plays an important role in photocatalytic reactions. Photoexcited charge carriers may behave similar to chemically donated charges. The higher binding energy of excess charges on the (011)-2 × 1 surface compared to those on the bulk or (110) surface implies that electron–hole separation and electron trapping is more efficient on the (011)-2 × 1 termination of rutile TiO<sub>2</sub>. This behavior contributes to the higher photocatalytic activity of the (011) surface for oxidation reactions,<sup>4–6</sup> and therefore, we propose this intrinsic mechanism to explain the previously reported face dependence of the photoactivity of TiO<sub>2</sub>. These observations imply that the photoactivity of TiO<sub>2</sub> may be tuned by appropriate crystal design. For example, composite materials with TiO<sub>2</sub> complexes with different coordination environments, like a square pyramid, could enhance photocatalytic activity.

## EXPERIMENTAL METHODS

Scanning tunneling microscopy (STM) and photoemission spectroscopy have been used to determine the origin of the band gap state in rutile TiO<sub>2</sub>(110) and (011) surfaces. The STM experiments were performed in an UHV chamber with base pressures in the low 10<sup>−10</sup> Torr range. The TiO<sub>2</sub> single crystals were cleaned by multiple cycles of Ar<sup>+</sup> sputtering at room temperature (1 kV, 5 μA, 30 min), followed by annealing at 650 °C for 15 min. The TiO<sub>2</sub> crystal was clip-mounted to a tantalum (Ta) sample plate, and the sample heater temperature was calibrated with a chromel–alumel thermocouple directly spot-welded to such a sample plate. STM imaging was done in constant current mode using an electrochemically etched tungsten tip. Empty-states STM images are shown throughout. The UPS data were measured at the 3 m TGM beamline at the Center for Advance Microstructures and Devices (CAMD) in Baton Rouge, LA. In the photoemission studies, TiO<sub>2</sub> samples with (110) and (011) orientations were mounted together on the same sample holder. This allowed a direct comparison of the two samples exposed to identical sample preparation conditions. Normal emission UPS spectra were recorded at an incidence angle of 45° with respect to the surface normal with a photon energy of 80 eV. The Fermi level was determined from the tantalum sample holder, which was in electrical contact with the sample.

## AUTHOR INFORMATION

### Corresponding Author:

\*To whom correspondence should be addressed. E-mail: mbatzill@usf.edu.

**ACKNOWLEDGMENT** We acknowledge financial support from the U.S. Department of Energy–Office of Basic Energy Sciences, Grant DE-SC0001508. Synchrotron studies were performed at the Center for Advanced Microstructure and Devices (CAMD) at Louisiana State University (LSU).

## REFERENCES

- (1) Borgarello, E.; Kiwi, J.; Grätzel, M.; Pelizzetti, E.; Visca, M. Visible Light Induced Water Cleavage in Colloidal Solutions of Chromium-Doped Titanium Dioxide Particles. *J. Am. Chem. Soc.* **1982**, *104*, 2996–3002.
- (2) Borgarello, E.; Kiwi, J.; Pelizzetti, E.; Visca, M.; Grätzel, M. Photochemical Cleavage of Water by Photocatalysis. *Nature* **1981**, *289*, 158–160.
- (3) Linsebigler, A. L.; Lu, G. Q.; Yates, J. T. Photocatalysis on TiO<sub>2</sub> Surfaces: Principles, Mechanisms, and Selected Results. *Chem. Rev.* **1995**, *95*, 735–758.
- (4) Hotsenpiller, P. A. M.; Bolt, J. D.; Farneth, W. E.; Lowekamp, J. B.; Rohrer, G. S. Orientation Dependence of Photochemical Reactions on TiO<sub>2</sub> Surfaces. *J. Phys. Chem. B* **1998**, *102*, 3216–3226.
- (5) Lowekamp, J. B.; Rohrer, G. S.; Hotsenpiller, P. A. M.; Bolt, J. D.; Farneth, W. E. Anisotropic Photochemical Reactivity of Bulk TiO<sub>2</sub> Crystals. *J. Phys. Chem. B* **1998**, *102*, 7323–7327.
- (6) Ohno, T.; Sarukawa, K.; Matsumura, M. Crystal faces of Rutile and Anatase TiO<sub>2</sub> Particles and Their Roles in Photocatalytic Reactions. *New J. Chem.* **2002**, *26*, 1167–1170.
- (7) Gong, X.-Q.; Khorshidi, N.; Stierle, A.; Vonk, V.; Ellinger, C.; Dosch, H.; Cheng, H.; Selloni, A.; He, Y.; Dulub, O.; et al. The 2 × 1 Reconstruction of the Rutile TiO<sub>2</sub>(011) Surface: A Combined Density functional Theory, X-ray Diffraction, and Scanning Tunneling Microscopy Study. *Surf. Sci.* **2009**, *603*, 138–144.
- (8) Torrelles, X.; Cabailh, G.; Lindsay, R.; Bikondoa, O.; Roy, J.; Zegenhagen, J.; Teobaldi, G.; Hofer, W. A.; Thornton, G. Geometric Structure of TiO<sub>2</sub>(011)(2 × 1). *Phys. Rev. Lett.* **2008**, *101*, 185501.
- (9) Kurtz, R. L.; Stockbauer, R.; Madey, T. E.; Roman, E.; Desegovia, J. L. Synchrotron Radiation Studies of H<sub>2</sub>O Adsorption on TiO<sub>2</sub>(110). *Surf. Sci.* **1989**, *218*, 178–200.
- (10) Zhang, Z.; Jeng, S.-P.; Henrich, V. E. Cation-Ligand Hybridization for Stoichiometric and Reduced TiO<sub>2</sub>(110) Surfaces Determined by Resonant Photoemission. *Phys. Rev. B* **1991**, *43*, 12004–12011.
- (11) Henrich, V. E.; Dresselhaus, G.; Zeiger, H. J. Observation of Two-Dimensional Phases Associated with Defect States on the Surface of TiO<sub>2</sub>. *Phys. Rev. Lett.* **1976**, *36*, 1335.
- (12) Henderson, M. A.; Epling, W. S.; Peden, C. H. F.; Perkins, C. L. Insights into Photoexcited Electron Scavenging Processes on TiO<sub>2</sub> Obtained from Studies of the Reaction of O<sub>2</sub> with OH Groups Adsorbed at Electronic Defects on TiO<sub>2</sub>(110). *J. Phys. Chem. B* **2003**, *107*, 534–545.
- (13) Wendt, S.; Sprunger, P. T.; Lira, E.; Madsen, G. K. H.; Li, Z.; Hansen, J. Ø.; Matthiesen, J.; Blekinge-Rasmussen, A.; Laegsgaard, E.; Hammer, B.; et al. The Role of Interstitial Sites in the Ti3d Defect State in the Band Gap of Titania. *Science* **2008**, *320*, 1755–1759.
- (14) Paxton, A. T.; Thiên-Nga, L. Electronic Structure of Reduced Titanium Dioxide. *Phys. Rev. B* **1998**, *57*, 1579–1584.
- (15) Di Valentin, C.; Pacchioni, G.; Selloni, A. Electronic Structure of Defect States in Hydroxylated and Reduced Rutile TiO<sub>2</sub>(110) Surfaces. *Phys. Rev. Lett.* **2006**, *97*, 166803.
- (16) Zhang, Z.; Yates, J. T. Effect of Adsorbed Donor and Acceptor Molecules on Electron Stimulated Desorption: O<sub>2</sub>/TiO<sub>2</sub>(110). *J. Phys. Chem. Lett.* **2010**, *1*, 2185–2188.
- (17) Diebold, U. The Surface Science of Titanium Dioxide. *Surf. Sci. Rep.* **2003**, *48*, 53–229.
- (18) He, Y.; Li, W.-K.; Gong, X.-Q.; Dulub, O.; Selloni, A.; Diebold, U. Nucleation and Growth of 1D Water Clusters on Rutile TiO<sub>2</sub>(011)-2 × 1. *J. Phys. Chem. C* **2009**, *113*, 10329–10332.

- (19) Yim, C. M.; Pang, C. L.; Thornton, G. Oxygen Vacancy Origin of the Surface Band-Gap State of  $\text{TiO}_2(110)$ . *Phys. Rev. Lett.* **2010**, *104*, 036806.
- (20) Guo, Q.; Cocks, I.; Williams, E. M. The Orientation of Acetate on a  $\text{TiO}_2(110)$  Surface. *J. Chem. Phys.* **1997**, *106*, 2924–2931.
- (21) Thevuthasan, S.; Herman, G. S.; Kim, Y. J.; Chambers, S. A.; Peden, C. H. F.; Wang, Z.; Ynzunza, R. X.; Tober, E. D.; Morais, J.; Fadley, C. S. The Structure of Formate on  $\text{TiO}_2(110)$  by Scanned-Energy and Scanned-Angle Photoelectron Diffraction. *Surf. Sci.* **1998**, *401*, 261–268.
- (22) Gutierrez-Sosa, A.; Martinez-Escolano, P.; Raza, H.; Lindsay, R.; Wincott, P. L.; Thornton, G. Orientation of Carboxylates on  $\text{TiO}_2(110)$ . *Surf. Sci.* **2001**, *471*, 163–169.
- (23) Bates, S. P.; Kresse, G.; Gillan, M. J. The Adsorption and Dissociation of ROH molecules on  $\text{TiO}_2(110)$ . *Surf. Sci.* **1998**, *409*, 336–349.
- (24) Käckell, P.; Terakura, K. Dissociative Adsorption of Formic Acid and Diffusion of Formates on the  $\text{TiO}_2(110)$  surface: the Role of Hydrogen. *Surf. Sci.* **2000**, *461*, 191–198.
- (25) Bao, S.; Liu, G.; Woodruff, D. P. Angle-Resolved Polarised Light Photoemission Study of the Formation and Structure of Acetate on  $\text{Cu}(110)$ . *Surf. Sci.* **1988**, *203*, 89–100.
- (26) Karis, O.; Hasselstrom, J.; Wassdahl, N.; Weinelt, M.; Nilsson, A.; Nyberg, M.; Pettersson, L. G. M.; Stohr, J.; Samant, M. G. The Bonding of Simple Carboxylic Acids on  $\text{Cu}(110)$ . *J. Chem. Phys.* **2000**, *112*, 8146–8155.
- (27) Krüger, P.; Bourgeois, S.; Domenichini, B.; Magnan, H.; Chandesris, D.; Fevre, P. L.; Flank, A. M.; Jupille, J.; Floreano, L.; Cossaro, A.; et al. Defect States at the  $\text{TiO}_2(110)$  Surface Probed by Resonant Photoelectron Diffraction. *Phys. Rev. Lett.* **2008**, *100*, 055501.
- (28) Thomas, A. G.; Flavell, W. R.; Mallick, A. K.; Kumarasinghe, A. R.; Tsoutsou, D.; Khan, N.; Chatwin, C.; Rayner, S.; Smith, G. C.; Stockbauer, R. L.; et al. Comparison of the Electronic Structure of Anatase and Rutile  $\text{TiO}_2$  Single-Crystal Surfaces Using Resonant Photoemission and X-ray Absorption Spectroscopy. *Phys. Rev. B* **2007**, *75*, 035105.